A GENERIC MODEL FOR RIDGES: A NEW FRAMEWORK TO CHARACTERISE BIOLOGICAL PLANAR STRUCTURES

Antonio Martinez-Sanchez[1] *Inmaculada Garcia*[2] *Jose-Jesus Fernandez*[3]

[1] Supercomputing and Algorithms Group, University of Almeria, 04120 Almeria, Spain
[2] Supercomputing and Algorithms Group, University of Malaga, 29080 Malaga, Spain
[3] National Centre for Biotechnology (CNB-CSIC), Campus UAM, 28049 Madrid, Spain

ABSTRACT

This work introduces a new generic framework to the analysis of ridges and its application to segmentation of planar structures in bioimaging. Based on a Gaussian model, local information associated to ridges is extracted, which actually characterise them. The theoretical basis of the framework is first presented for the one-dimensional case. Its extension to higher dimensions is then shown to be straightforward by applying the same basis over the maximum curvature direction. In the particular case of 3D, this framework allows characterisation of planar structures. The potential of the methodology to segment planar structures in 3D bioimaging is illustrated with several examples.

Index Terms— Biomedical image processing, Image analysis, Image segmentation, Image classification, Computed tomography

1. INTRODUCTION

The differential structure of images was established in the 90s [1]. They defined the concept of scale and determined how to use differential geometry tools, such as gradient and curvature, to describe image structure. The concept of *isophote*, which allows describing objects as manifolds, also comes from those works. Edges and ridges can be described as 1-manifolds (curves in the plane) in images and 2-manifolds (surfaces in the space) in volumes (tomograms). Nowadays, they are widely used tools in image processing [2, 3, 4].

Ridges are very useful in Computer Vision. For example, they are used to detect and analyse blood vessels [5] or others tube-like [6] or plane-like [7] structures in biomedical data, to study objects in structural biology [8] or to analyse fingerprints [9]. Ridge detection extracts topological and certain geometrical information of structures and this information can be used for detecting patterns.

Structures that can be considered as ridges at local scale are often found in bioimaging datasets. In this work we focus only on plane-like structures, and biological membranes are one of the best examples. Membranes encompass compartments within biological specimens, define the limits of the intracellular organelles and the cells themselves. However, in most cases ridge detection is not enough for membrane characterisation. For example, external and internal membrane separation in organelles is a typical task in structural biology [10] and nowadays there is not a generic method for doing that. In most cases, membranes can be characterised by analysing only the local information. However, problems arise because classical ridge detectors, based on differential geometry, do not carry out an exhaustive analysis of the local information. Some previous works tried to extract extra local information from ridges to solve particular problems, e.g. thickness estimation of tube structures such as blood vessels [3, 11], or plane structures such as cortices or articular cartilages [7]. However, these proposals are not generic enough for recovering local information from ridges in grey-scale data.

This work describes a new generic framework for studying the local information associated to ridges in order to improve the characterization of planar structures in bioimaging datasets. As a result, the segmentation of these data can be performed or improved. Furthermore, the parameters used to describe the local information of ridges are associated with features visually perceptible by humans. Consequently, these parameters directly solve some segmentation problems or can be used for further assisting human supervision.

2. THEORETICAL ANALYSIS

This section shows how ridges, local maxima, can be locally described in a one-dimensional function. In that case a ridge is a 0-manifold (a point in $\mathbb{R}$). Then, this development is used as the base of $(d-1)$-manifolds descriptions in $\mathbb{R}^d$.

2.1. 1D data

This work assumes that the information of interest, i.e. foreground, is represented by positive curvature structures

Work partially supported by the Spanish Ministry of Science (TIN2008-01117) and J. Andalucia (P10-TIC-6002), in part financed by the European Reg. Dev. Fund (ERDF). A.M.S. is a fellow of the Spanish FPI programme.

whereas those with negative curvature represent the background. Therefore, local maxima, ridges, in 1D allow isolation of the set of so-called DOI (*Details Of Interest*) $\mathcal{D} = \{x_j : j = 1, ..., K_{\mathcal{D}}\}$, where x_j is a 0-manifold. A simple Gaussian-based model can be used to locally describe every detail. This model is defined as $f_m : \mathbb{R} \to \mathbb{R}^+$:

$$f_m(x) = o_j + s_j \exp\left(-\frac{(x - x_j)^2}{2t_j^2}\right) \tag{1}$$

where x_j is a element of DOI, o_j (*offset*) represents its intensity level offset, s_j is the local significance (*sharpness*) and the width is expressed by t_j (*thickness*). The function f_m is a local approximation of f. Consequently we must establish what is local for every $x_j \in \mathcal{D}$. The next three premises have been used so as to establish local sets, $\mathcal{E}$:

- $x_j \in \mathcal{E}_j \Rightarrow x_j \notin \mathcal{E}_i, \forall i \neq j$ where $i, j \in \{1, 2, \cdots, K_{\mathcal{D}}\}$
- $\mathcal{E}_j \cap \mathcal{E}_i = \emptyset, \forall i \neq j$ where $i, j \in \{1, 2, \cdots, K_{\mathcal{D}}\}$.
- $\bigcup_1^{K_{\mathcal{D}}} \mathcal{E}_j = X - \left\{\bigcup_1^{K_{\mathcal{S}}} \mathcal{S}_i\right\}\ \forall j \in \{1, ..., K_{\mathcal{D}}\}$ and $\forall i \in \{1, ..., K_{\mathcal{S}}\}$, where $\mathcal{S}_i$ is one of the $K_{\mathcal{S}}$ *step* regions that are pure edges and that do not contain relevant information and cannot be adjusted by f_m.

If we divide X through *antidetails* we will get a consistent solution with the previously defined premises. In this paper antidetails are such $\mathcal{G} = \{x_g : g = 1, ..., K_{\mathcal{G}}\}$ that:

$$\frac{\partial f(x)}{\partial \vec{v_{x_j}}} = 0 \quad \forall x \in (X - \mathcal{D}) \tag{2}$$

where $\vec{v_{x_j}} = (x - x_j)/||x - x_j||$. According to this, the details have to be calculated before the antidetails.

Except for the special cases of $j = 1$ and $j = K_{\mathcal{D}}$, a detail x_j is delimited by the antidetails x_j^l and x_j^r. Consequently $\mathcal{E}_j = [x_j^l, x_j^r] \supset x_j$. For the special cases of $j = 1$ and $j = K_{\mathcal{D}}$, $\mathcal{E}_1 = [\inf\{X\}, x_1^r] \supset x_1$ and $\mathcal{E}_{K_{\mathcal{D}}} = [x_{K_{\mathcal{D}}}^l, \sup\{X\}] \supset x_{K_{\mathcal{D}}}$, where $\inf\{\cdot\}$ and $\sup\{\cdot\}$ are respectively the infimum and superior of a set. Using antidetails, the step regions can be isolated as well. Figure 1 shows that data on the left and right side of a detail are not necessarily symmetrical. However, the Gaussian model in Eq. (1) is symmetrical. To accommodate this asymmetry, the model is then divided in two parts, so that we end up with the next piecewise function

$$f_{mp} = \begin{cases} f_l = f_m(x^l) & \forall x^l \in [x_j^l, x_j] = \mathcal{E}_j^l \\ f_r = f_m(x^r) & \forall x^r \in [x_j, x_j^r] = \mathcal{E}_j^r \end{cases} \tag{3}$$

for every detail x_j. The previous definition of $\mathcal{E}_j = \mathcal{E}_j^l \cup \mathcal{E}_j^r$ also allows the introduction of a new pair of parameters, *resolution*, that are calculated by $r_j^l = \varnothing\left\{\mathcal{E}_j^l\right\}$ and $r_j^r = \varnothing\left\{\mathcal{E}_j^r\right\}$, where $\varnothing\{\cdot\}$ is the diameter of a set. Now, the value

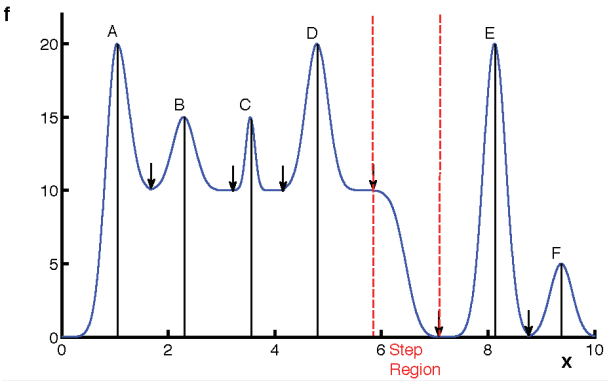


Fig. 1. Six ridges with different properties in 1D. Their description in terms of model parameters is in Figure 2.

of the parameter $p_j \in (o_j, s_j, t_j, r_j)$ is established as $p_j = \max\left\{p_j^l, p_j^r\right\}$.

The definition of $\mathcal{E}_j = \mathcal{E}_j^l \cup \mathcal{E}_j^r$ also leads us to add asymmetry parameters, a_j^p (*asymmetry of p*), which will allow us to completely describe the morphology of a detail. In general, the asymmetry can be expressed as

$$a_j^p = \frac{|p_j^l - p_j^r|}{|p_j^l + p_j^r|} \tag{4}$$

to preserve all the detail information. Special cases are the asymmetry for offset and sharpness because both are interrelated. Therefore their asymmetry is calculated by:

$$a_j^o = \frac{|o_j^l - o_j^r|}{|o_j + s_j|} \quad a_j^s = \frac{|s_j^l - s_j^r|}{|o_j + s_j|} \tag{5}$$

Once every detail and its local neighbourhood has been detected, the model parameters can be adjusted, f_{mp} (Figure 2). Model fitting can be expressed as an overdetermined non-linear equations system over the space $I_j \subset \mathbb{R}^{+6}$:

$$\underset{\bar{o}_j, \bar{s}_j, \bar{t}_j}{\arg} \left[\min\left\{\sum_{\forall k} (f(x_k) - f_{mp}(x_k; \bar{o}, \bar{s}, \bar{t}))^2\right\}\right] \quad \forall x_k \in \mathcal{E}_j \text{ and } [\bar{o}_j, \bar{s}_j, \bar{t}_j] \in I_j \tag{6}$$

An optimization algorithm can solve this problem and the result consists of a set of parameters for f_{mp} that minimises the quadratic error (Figure 2(right)). A new parameter can then be added to describe a ridge, namely *adjustment*:

$$q_j^l = \frac{E_j^l}{r_j^l} \quad q_j^r = \frac{E_j^r}{r_j^r} \tag{7}$$

where E_j^i is the quadratic error of the model fitting for the detail j in the subset $\mathcal{E}_j^i$ and $i \in (l, r)$.

2.2. $\mathbb{R}^d$ data

The theoretical basis of this method has just been described for 1D signals. For data from a d-dimensional space with

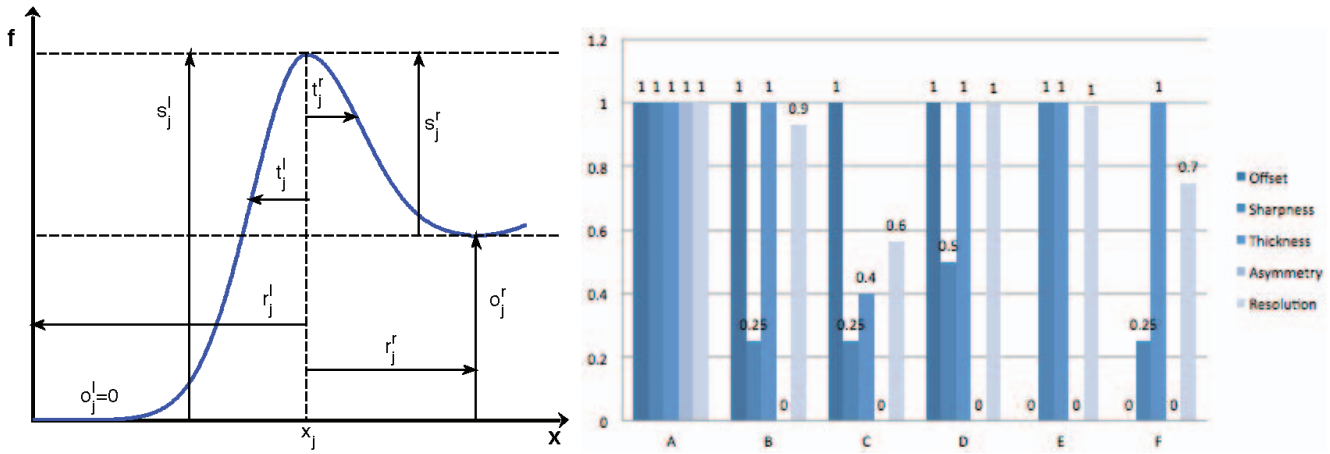


Fig. 2. (left) Scheme of ridge A in Fig. 1 and its parameters. (right) Model parameters for ridges in Fig. 1, normalized in $[0, 1]$.

$d > 1$ (i.e. 2D for images; 3D for tomograms), an extension of a local maximum can be a ridge described as a $(d-1)$-manifold (*plane ridge*) [12] (there are other types of ridges described by others manifolds, but they are not considered in this work). As a result, a point $x_j \in \mathbb{R}^d$ in a ridge (detail) can be defined by its second order differential structure. Therefore every point in a ridge fulfils the next conditions:

$$\begin{cases} D\left(f(x_j)\right) \cdot \vec{v_1} = 0 \\ \lambda_1 < 0 \\ \lambda_i \geq 0 \; \forall i \in \{2, 3, \cdots, d\} \end{cases} \tag{8}$$

where $D() \cdot \vec{v}$ is the directional derivative in direction $\vec{v_1}$, λ_1 and λ_i are the eigenvalues of Hessian matrix in x_j, where $|\lambda_1| \geq |\lambda_i|$, and $\vec{v_1}$ is the corresponding eigenvector to λ_1 [10]. Note that $\vec{v_1}$ is the direction of the maximum curvature.

These ridges can thus be described by studying f in the $\vec{v_1}$ direction because the local maximum only exists in that direction. This property allows us to convert the function $f : \mathbb{R}^d \rightarrow \mathbb{R}^+$ into a 1D function, $\overline{f} : \mathbb{R} \rightarrow \mathbb{R}^+$, in the neighbourhood, $\mathcal{E}_j$, of the detail x_j. Consequently, the theory developed in the previous subsection for 1D data can be applied here. Then $\overline{f}$ is adjusted to f_{mp} and its parameters will allow to describe the detail, x_j, that is part of a $(d-1)$-manifold in $\mathbb{R}^d$.

3. EXPERIMENTAL RESULTS

This framework has been tested with tomograms and images taken under different experimental conditions and from different specimens. The characterisation of ridges is then used for segmentation purposes. The segmentation results presented here have been post-processed by a simple thresholding of the ridge model parameters, followed by a hysteresis process and a simple global analysis based on size [10].

3.1. Mouse heart tissue

The first test dataset was a 3D tomogram from adult mouse myocardium [13] (Figure 3). It presents complex structures densely packed that proved to be difficult to be separated by standard generic algorithms. For this reason this kind of tomograms is usually segmented by hand by human experts. However, the framework presented here lets us classify the plane structures according to their local ridge properties (Figures 3 and 4) because it exploits all local information in contrast to descriptors based on classic differential analysis tools [10]. As shown in Figure 3(right), offset, sharpness and thickness greatly contributed to the classification of the structural components.

3.2. Mitochondrion

A tomogram of a neuronal mitochondrion [14] with poorer signal-to-noise ratio was tested as well. Our framework to locally describe membranes succeeds in delineating the outer membrane and inner cristae and segmenting them as separated objects (Figure 4). In this particular case, the asymmetry parameter played a central role in the separation of the outer (yellow-bright) and inner (red-dark) planar features. This tomogram was also segmented in [10] by an algorithm based on differential geometry. However, in that work a global analysis stage based on size was not able to discriminate completely the external membrane from the inner planar cristae.

4. CONCLUSION

A new framework for the study of the local information associated to ridges, and its extension to planar structures in 3D datasets, have been presented. The methodology relies on the characterisation of ridges by means of a set of parameters according to an asymmetrical Gaussian model. The extension to higher dimensions stems from the analysis along the maximum curvature direction. The segmentation process to be applied next is improved thanks to the local information wealth provided by this framework. The results with experimental datasets have clearly shown the good performance for segmentation of planar structures even in noisy and distorted

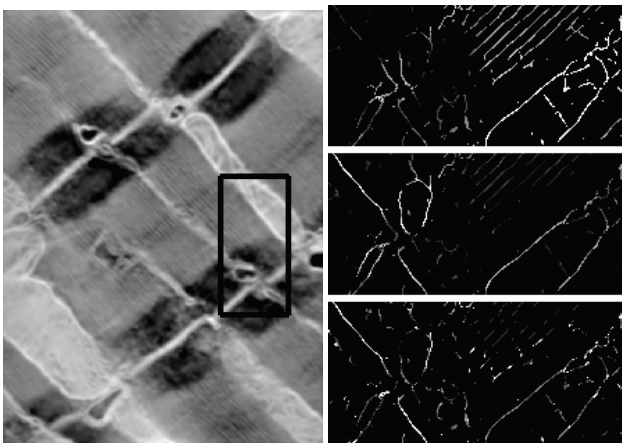


Fig. 3. (left) Slice from the mouse heart tissue tomogram. (right) Some ridge model parameters on the area sketched in left, after zoom and rotation (-90^o); offset (top), sharpness (centre) and thickness (bottom).

environments. Moreover, it has been proved that a relatively simple segmentation algorithm (e.g. thresholding) can handle complex bioimaging data. Therefore, the potential of this framework could be exploited as a pre-processing stage of any segmentation algorithm that deals with plane structures.

5. REFERENCES

[1] L. Florack, B. Romeny, J. Koenderink, and M. Viergever, "Scale and differential structure of images," *Image Vis. Comp.*, vol. 10, pp. 376–388, 1992.

[2] M. Jacob and M. Unser, "Design of steerable filters for feature detection using canny-like criteria," *IEEE TPAMI*, vol. 26, no. 8, pp. 1007–1019, 2004.

[3] T. Pock, R. Beichel, and H. Bischof, "A novel robust tube detection filter for 3d centerline extraction," *LNCS*, vol. 3540, pp. 55–94, 2005.

[4] P. Arbeláez, M. Maire, C. Fowlkes, and J. Malik, "Contour detection and hierarchical image segmentation," *IEEE TPAMI*, vol. 33, no. 5, pp. 898–916, 2011.

[5] C. Kirbas and Q. Francis, "A review of vessel extraction techniques and algorithms," *ACM Comput. Surv.*, vol. 36, pp. 81–121, 2004.

[6] C. Bauer, T. Pock, E. Sorantin, H. Bischof, and R. Beichel, "Segmentation of interwoven 3d tubular tree structures utilizing shape priors and graph cuts," *Medical Image Anal.*, vol. 14, no. 2, pp. 172–184, 2010.

[7] Y. Sato, H. Tanaka, T. Nishii, K. Nakanishi, N. Sugano, T. Kubota, H. Nakamura, H. Yoshikawa, T. Ochi, and S. Tamura, "Limits on the accuracy of 3d thickness measurement in MR images-effects of voxel anisotropy," *IEEE TMI*, vol. 22, pp. 1076–1088, 2003.

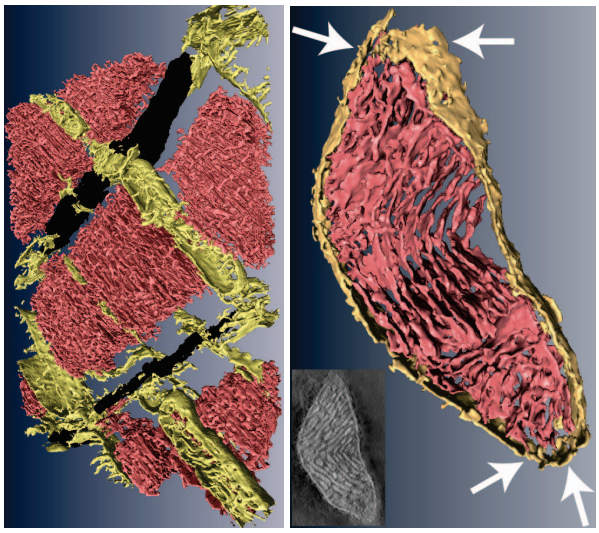


Fig. 4. 3D segmentation from ridge model parameters. (left) Mouse heart tissue where its plane structures are classified; T-tubes, sarcoplasmic reticulum and vicinal mitochondria (yellow-bright), myosin fibres (red-dark) an Z-lines (black). (right) Segmentation of external membrane (yellow-bright) and internal plane structures (red-dark) of a neuronal mitochondrion. Arrows point to external membrane regions that [10] misclassified. Inset: slice of the original tomogram.

[8] Z. Yu and C. Bajaj, "A structure tensor approach for 3d image skeletonization: Applications in protein secondary structure analysis," in *IEEE ICIP*, 2006, pp. 2513–2516.

[9] N. Yager and A. Amin, "Fingerprint classification: a review," *Pattern Anal. & App.*, vol. 7, pp. 77–93, 2004.

[10] A. Martínez-Sánchez, I. García, and J. Fernández, "A differential structure approach to membrane segmentation in electron tomography," *J Struct Biol*, vol. 175, pp. 372–383, 2011.

[11] J. Lowell, A. Hunter, D. Steel, A. Basu, R. Ryder, and R.L. Kennedy, "Measurement of retinal vessel widths from fundus images based on 2-d modeling," *IEEE TMI*, vol. 23, no. 10, pp. 1196–1204, 2004.

[12] D. Eberly, "Fast algorithms for ridge construction," *Proceedings SPIE Photonics*, vol. 2356, pp. 231–242, 1994.

[13] T. Hayashi, M. Martone, Z. Yu, A. Thor, M. Doi, M. Holst, M. Ellisman, and M. Hoshijima, "Three-dimensional electron microscopy reveals new details of membrane systems for ca2+ signaling in the heart," *J Cell Sci*, vol. 122, pp. 1005–1014, 2009.

[14] G. Perkins, C. Renken, M. Martone, S. Young, M. Ellisman, and T. Frey, "Electron tomography of neuronal mitochondria," *J Struct Biol*, vol. 119, pp. 260–72, 1997.